Desalination and Water Treatment
www.deswater.com

doi: 10.5004/dwt.2022.28678

267 (2022) 89–97
August

Experimental research of turbulence kinetic and water force acting on spur dike

Tao Yu[a,b,*], Qiuqian Duan[a,b], Pingyi Wang[a,b], Linfeng Han[a,b]

[a]*National Engineering Research Center for Inland Waterway Regulation, Chongqing Jiaotong University, Chongqing 400074, China, email: yutaochq@sina.com (T. Yu)*
[b]*Key Laboratory of Hydraulic and Waterway Engineering of the Ministry of Education, Chongqing Jiaotong University, Chongqing 400074, China*

Received 27 April 2021; Accepted 10 July 2022

ABSTRACT

The waterlogging phenomenon of spur dike as a common type of waterway regulation building is very common. In this article, turbulence and mechanics research around the spur dike was carried out through physical model experiment; which illuminates the turbulence and Karman Vortex of spur dike erosion, the influence of pulsation kinetic energy is established and the corresponding relationship between pulse pressure and local scour, analyzed the Karman Vortex and the relationship between the dike after flushing, the influence of different influencing factors (discharge, water depth, bottom slope, length of spur dike) on the force of spur dike is systematically analyzed. The research results are of great significance for understanding the mechanism of scour and failure of spur dikes, and can provide reference for the design of spur dikes.

Keywords: Spur dike; Turbulence kinetic; Karman Vortex; Scour mechanism

1. Introduction

As a kind of waterway regulation building, the spur dike has the function of harnessing water to attack sand, raising upstream water level and improving waterway flow conditions. The layout of the groin dike has changed the local water surface conditions and water flow pattern of the original waterway, and has been widely used in waterway regulation projects [1]. Since H. Engels, a famous expert in hydraulic engineering, made the experiment in the early 1920s, many scholars have also conducted specialized experimental studies, one of which is to determine the maximum depth of the dike head. For example, in Makavyevov's formula [2], the line near velocity, the Angle between the axis of water flow and the axis of the spur dike, the acceleration of gravity and the particle size of bed sand are taken as the influencing factors, while in Siow-Yonglim and Ye-Mengchiew's formula [3], the Froude number, dike length, particle size of bed sand and water depth are taken as the influencing factors. In the formula of Ying [4], the dike length, average water depth, maximum velocity of the dike head and the initial velocity of sediment are taken as the influence factors. In the formula of Fang and Wang [5], the concept of the impact velocity of the dike head is introduced.

Uijttewaal [6] concluded through physical model tests that subtle changes in the design of the spur dike would have complex influences on the interaction between water flows, the shape of the riverbed and sediment transport, etc. Mostafa et al. [7] and Ahmed et al. [8] concluded through moving bed tests that the water depth at the center line of the main channel of the permeable dike would not change, while the water depth at the center line of the main channel of the solid dike would change to some degree. Xu et al. [9] studied the variation rule of water surface line with void ratio and void size of pervious groin through flume test. Yu et al. [10] conducted an experimental study on the

* Corresponding author.

1944-3994/1944-3986 © 2022 Desalination Publications. All rights reserved.

stability of different types of spur dikes through physical models. Zhong et al. [11] studied the turbulence characteristics of the flow in a tightly arranged rough bed open channel through the turbulent PIV flow field test data. Wang et al. [12] analyzed the distribution law of flow turbulence intensity, Reynolds stress and turbulence kinetic energy in a wide and narrow channel through an indoor generalized model test. Kumar and Ojha [13] studied the turbulence characteristics of non-submerged hook groin through model tests and obtained the relationship between the turbulence kinetic energy and the shear stress on the bed surface.

All the above formulas take the average flow velocity as one of the limiting factors of scour, ignoring the existence of flow turbulence and vortex near the dike head, and the existing research results show that turbulence has a great influence on scour. Therefore, the relationship between pulsating kinetic energy and pressure and dike scour is analyzed from the point of view of flow turbulence, and it is pointed out that the Karman Vortex makes an important contribution to the formation of dike head scour pit and the backflow area behind the dike, which is of guiding significance for further understanding the mechanism of dike local scour and improvement of dike head scour depth formula.

2. Experiments

The clear water scouring Experiment was conducted in a glass flume in length of 30 m and width of 2 m. The maximum scour depth of prototype spur dike is about 10 m, and the average depth of the scour pit is about 7 m. According to model scale, its quartz sands were laid on the middle of the flume in thickness of 0.3 m and length of 15 m (Fig. 1). The layout of measurement positions and the spur dike is shown in Fig. 2.

Three kinds of spur dikes with different lengths were designed in the model test. The width of the spur dikes crest was 5 cm, the height was 10 cm, and the length was 20, 30, and 50 cm respectively. The slope of the upstream is 1:1.5, the downstream is 1:2, and the river slope is 1:5. The head of the spur dike is a circular arc.

The test was carried out with the spur dike just flooded. Quartz sand was selected as the model sand in this experiment, with bulk density γ_s = 2.65 t/m^3 and D_{50} = 0.18 mm.

In order to study the hydrostatic pressure, hydrodynamic pressure and pulsation pressure at different positions of the spur diver, nine measuring sections were set up around the spur diver. Three pressure test sections are set up in the upstream, downstream and end of the spur dike respectively, and three sampling points are set up in each section. When the length of the groin is 20 or 30 cm, delete 1# and 9# pressure measurement sections; three pressure measuring sections are arranged at the head of the spur dike.

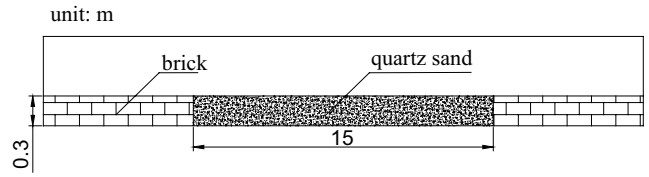

Fig. 1. Layout of the model test.

Adopts Japan 3066 high precision manometer to automatically record the pressure, the error can be guaranteed within 5%. Using acoustic Doppler velocimeter to measure the flow velocity, the error can be guaranteed within 3%. In this experiment, it is necessary to observe the flow turbulence under various working conditions, as well as the distribution of the total water pressure and the total pulsation pressure at each measuring point.

3. Analysis

3.1. Relationship between turbulent motion and scouring near the spur dike

Use u as instantaneous velocity of flow, $\bar{u}$ as time averaged instantaneous velocity of flow, σ_u as mean square deviation of instantaneous velocity of flow, u' as fluctuating velocity, so mean square deviation of fluctuating velocity is just the flow turbulence intensity [7], that is $\sigma_{u_i} = \sqrt{\frac{1}{n}\sum_{j=1}^{n} u_j'^2}$. If η is flow pulsation kinetic-energy, then pulsation kinetic-energy of one point can be expressed as $\eta_i = \frac{1}{2}\left(2\sigma_{u_i}\right)^2$, that is, $\eta_i = 2\sigma_{u_i}^2$.

Taking test condition of Q = 38.7 L/s, L = 50 cm and H = 12cm (where Q is the flow, L the length of the spur dike, and H the water depth) for example, it can explain the relationship among pulsation kinetic-energy, fluctuating pressure of flow and the scour hole behind the spur dike. The distribution of the pulsation kinetic-energy and the fluctuating pressure are shown in Figs. 3 and 4; Fig. 5 is the topographic map of scouring end. The line of X = 0 coincides with the axis of the spur dike in Figs. 3–5. The unit of contour value in Figs. 3 and 4 is respectively Joule and kilopascal. The unit of contour value in Fig. 5 is meter, where negative value is scour depth and positive value is silting-up [14–16].

In the upstream of the spur dike, fluctuating velocity is lower, the value of the fluctuating pressure and pulsation kinetic-energy is smaller, and flow turbulence intensity is weaker, so little scouring occurs in upstream of the spur dike. Near the opposite bank of the spur dike, although unit width flow and velocity being increased, the value of the fluctuating pressure and pulsation kinetic-energy not increased any more, so flow turbulence intensity is still weaker and scouring is also less. With the increasing of fluctuating pressure and pulsation kinetic-energy, there is a strong turbulent motion area near the spur dike end where sediment can easily be started up and be carried away by the flow. So, scouring is widespread and the value of the fluctuating pressure and pulsation kinetic-energy is up to the maximum in this area, where is the core of the flow turbulence and pressure pulsation (Figs. 3 and 4). What we can discover from Figs. 3–5 is that: (1) the flow turbulence core appears in the area of 0.2 m < X < 1.0 m, 0.6 m < Y < 1.1 m; (2) the pressure pulsation core appears in 0.2 m < X < 1.1 m, 0.8 m < Y < 1.1 m; (3) scour hole appears in 0.1 m < X < 0.8 m, 0.8 m < Y < 1.2 m. It is concluded that these three zones are about the same, and the zone where the pulsation kinetic-energy and fluctuating pressure are up to maximum is almost where it is scoured the most seriously [8].

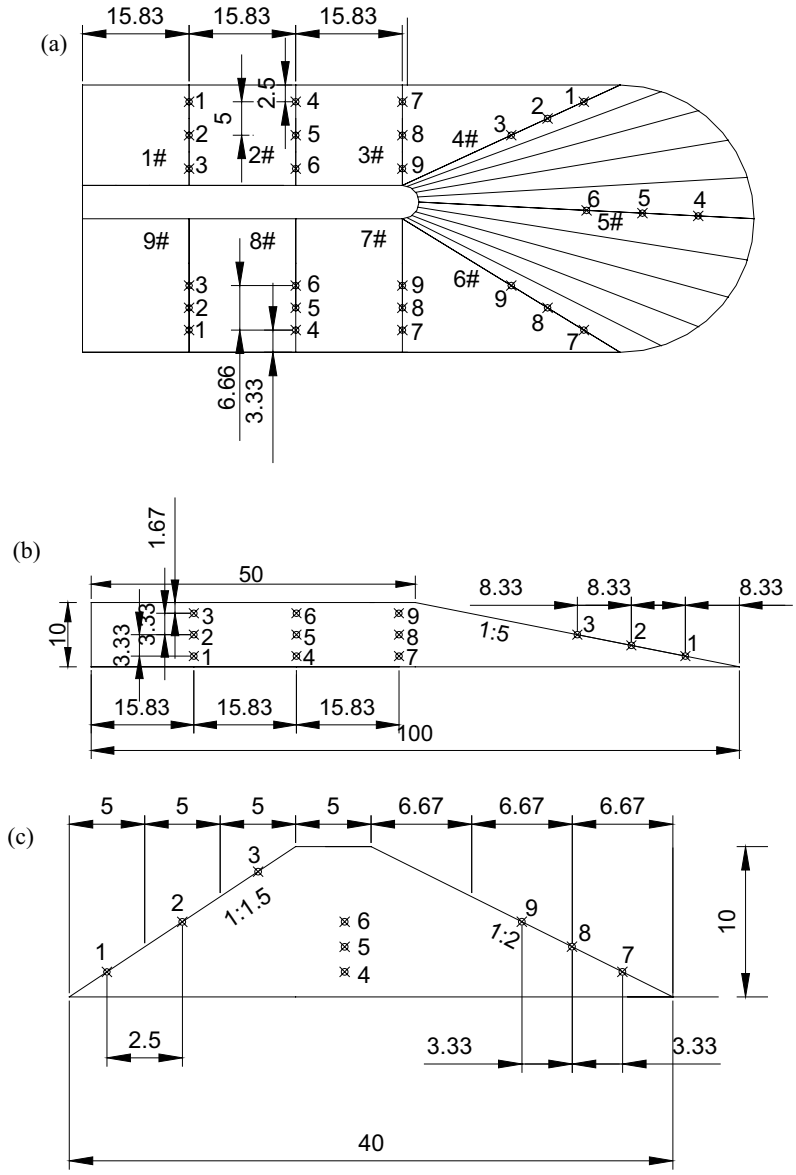

Fig. 2. The layout of measurement positions and the spur dike. (a) Horizontal view of measurement positions and the spur dike body (unit: cm), (b) lateral view of measurement positions and the spur dike (unit: cm) and (c) vertical view of measurement positions and the spur dike (unit: cm).

3.2. Relationship between Karman Vortex and scouring near the spur dike end

When a fluid particle flow in front of the un-streamlined cylinder, the pressure of which would elevate from the flow pressure to the stagnation pressure, and the high pressure flow close to the edge impel the developing overlaying bed to the both sides of the cylinder. But when the Reynolds number is big enough, the force produced by pressure is insufficient to push overlaying bed to surround the back of the bluff body. The overlaying bed in the surface of the cylinder fell off from both sides near the biggest cross-section of the cylinder, forming two shear layers, which is towed to the end in the flow. These two free shear layers become the boarder of the wake. Since the innermost free shear layer moves more slower than the outer layer contacting with free flow, these shear layers are prone to coil a discontinuous rotational vortex, and in the wake, it forms a regular flow pattern vortex [9,10]. With the increasing of the Reynolds number, one of the vortexes detached from the cylinder, and the periodic wake and staggered vortex tract are formed; this is so called Karman Vortex Street. The genesis and development of this vortex have regular pattern; with its generation, the fluid vibration can occur around and downstream the object. Vibration frequency is proportional to flow velocity. This phenomenon can be observed by moving flagpole and flag due to the wind [17–19].

By observing and analysis of the experimental phenomenon, Reynolds number within a certain range, when the flow bypass arc-type groin head (one side of the cylinder),

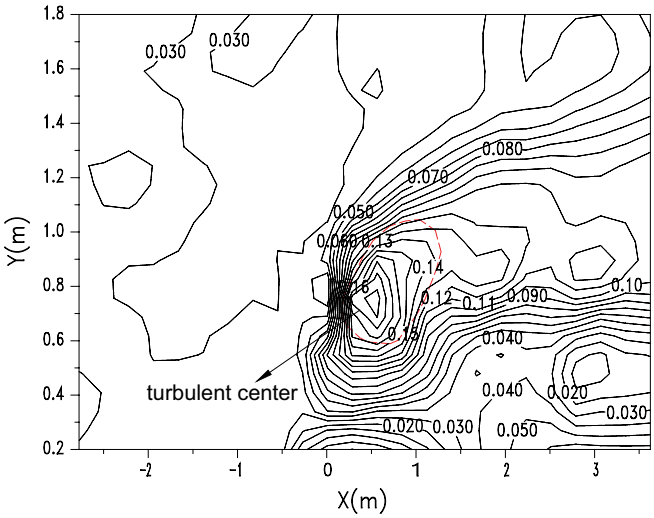

Fig. 3. Distribution of the pulsation kinetic energy.

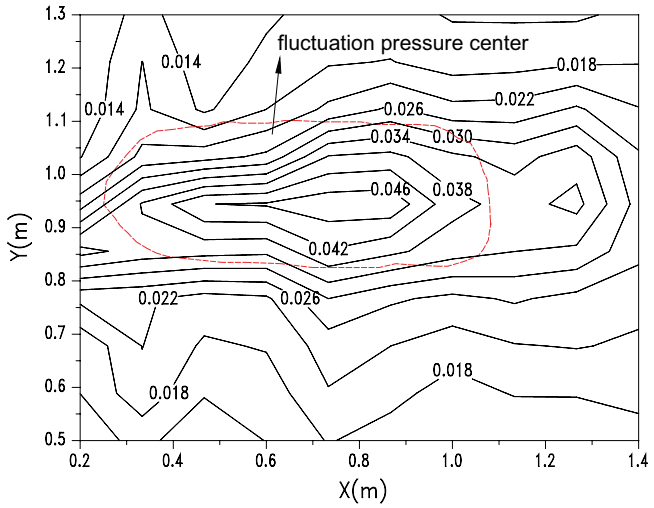

Fig. 4. Distribution of the fluctuating pressure.

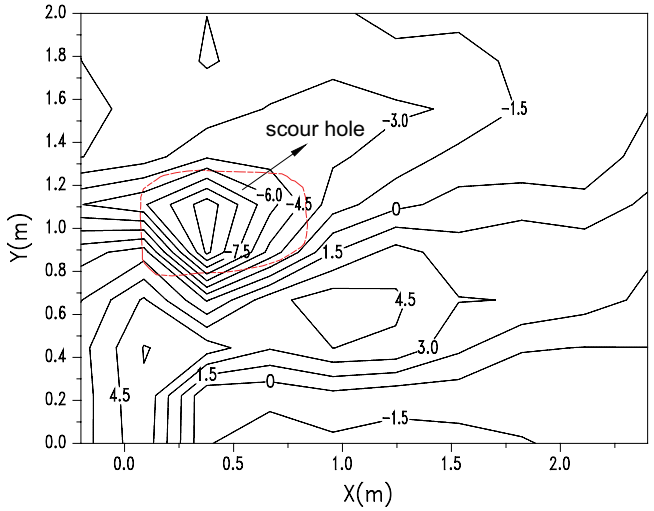

Fig. 5. Final scouring terrains.

uniseriate Karman Vortex could occur. The shape of Karman Vortex behind the vertical cylinder is funneled; The slope of the curved surface of the groin head is 1:5, so the shape of the three dimensional Karman Vortex above it is also funneled, but its Vortex axis is of an oblique and nonholonomic circle.

Strouhal proposed Strouhal Number (fd/v) through research which is dimensionless [11,12], where f is the vortex frequency, d is the diameter of cylinder, v is flow velocity. As Reynolds number being in the range of 3×10^2 to 2×10^5, Strouhal Number would be a constant value and its numerical value is about 0.2. It can be expressed as:

$$f = \mathrm{St}\frac{v}{d} \approx 0.2\frac{v}{d} \tag{1}$$

where St is Strouhal Number.

Rotation direction of vortex behind the cylinder just can be shown in Fig. 6. One side is clockwise, and another is counter-clockwise. Suppose the distance between vortex streets is h, the space between vortex is l, it has been proved by Von Kalman and can be derived as follows:

$$\sin\left(\pi h / l\right) \text{ Or } h / l = 0.281 \tag{2}$$

The two Parallel vortex rows, shown in Fig. 6, have the same circulation, Γ and –Γ, (the circulation Γ is vortex intensity). As it can be seen as the product of the average value of the velocity and length of a closed curve in fluid, it can be expressed as

$$\Gamma = \int_C v_s ds = \iint \left(\mathrm{rot}\vec{v}\right)_n ds = 2\pi R v_s \tag{3}$$

where $\vec{v}$ is velocity vector, rot$\vec{v}$ is rotor, R is radius of the moving vortex, v_s is tangential velocity on the brink of the vortex.

Based on research findings by our predecessors, relationships between d and h, Γ and v, can be written as:

$$h = 1.3d \tag{4}$$

$$v = \frac{\Gamma}{0.28\sqrt{2l}} \tag{5}$$

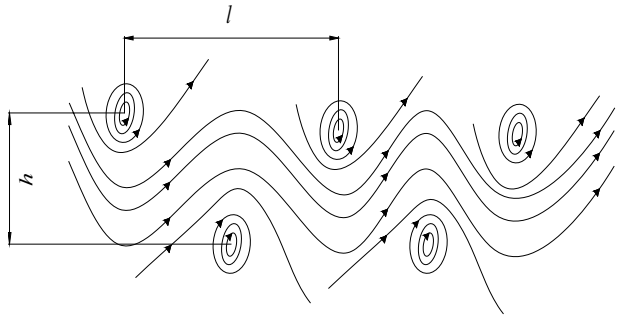

Fig. 6. Asymmetric Vortex Street alternately arranged behind the cylinder.

As the resultant velocity of the approach velocity and linear velocity on the brink of the vertex is faster than the incipient velocity of sediment, bed sediment can start up and the river bed is scoured. It can be expressed as:

$$v \pm v_s > u_c \tag{6}$$

$$u_c = \lg \frac{8.8H}{D_{95}} \sqrt{\frac{(\gamma_s - \gamma) g D_{50}}{3.5\gamma}} \tag{7}$$

where u_c is sediment incipient velocity, which can be obtained by Gang Chalov formula [13].

Taking test condition of Q = 38.7 L/s, L = 50 cm and H = 10 cm for example, the relationship among Karman Vortex, sediment incipient motion and scour behind the spur dike can be studied. In this condition, since approach velocity is 0.216 m/s, the diameter of circular groin head is 0.4 m, radius of the moving vortex is in the range of 0.15–0.25 m based on test observation, here R is 0.2 m, then:

By Eq. (4) $h = 1.3d = 1.3 \times 0.4 = 0.52m$

By Eq. (2) $l = h / 0.281 = 0.52 / 0.281 = 1.851m$

By Eq. (5) $\Gamma = 0.28\sqrt{2}lv = 0.158m^2 / s$

By Eq. (3) $v_s = \frac{\Gamma}{2\pi R} = \frac{0.158}{2 \times 3.14 \times 0.2} = 0.126m$

By Eq. (7) $u_c = \lg \frac{8.8H}{D_{95}} \sqrt{\frac{(\gamma_s - \gamma) g D_{50}}{3.5\gamma}} = 0.219m / s$

Karman Vortex behind the spur dike end is clockwise (Fig. 7). The resultant velocity, approaching the brink of the vortex in the main flow zone, is $v + v_s$ = 0.342 m/s > u_c = 0.219 m/s. The resultant velocity, near the brink of the vortex in the backflow zone behind the spur dike, is $v - v_s$ = 0.09 m/s < u_c = 0.219 m/s. That is to say, the resultant velocity approaching the brink of the vortex in the main flow zone is greater than sediment incipient velocity, so bed sediment can start up and the scour pit near the spur dike is engendered; the resultant velocity near the brink of the vortex in the backflow zone behind the spur dike is less than sediment incipient velocity, so bed sediment cannot start up, with the vortex moving, some sediment can be taken to this zone and deposits, forming longitudinal dune [20,21].

3.3. Influencing factor force on spur dike body

The test results show that the total pressure and hydrodynamic pressure at each measuring point are related to the length, discharge, water depth and the bottom slope of the spur dike, but the relationship between the average period and frequency and each factor is negligible.

3.3.1. Influence of flow rate on the force of spur dike

When the length of the spur dike is 30 cm, the water depth is 10 cm, and the flow rates are 25.8, 38.7, 51.0, and 68.0 L/s, the stress conditions of 8 sampling points 1.67 cm away from the bottom of the flume are compared and analyzed. The relationship between the total pressure and the flow rate of the groin is shown in Table 1 and Fig. 8.

The relationship between hydrodynamic pressure and flow rate is shown in Table 2 and Fig. 9.

It can be seen from Table 1 and Fig. 8 that the flow rate has little influence on the upstream total pressure of the spur dike, but with the increase of the flow rate, the total pressure at the end of the spur dike and the downstream presents a downward trend. The reason is that the water depth controlled in the test is located upstream of the spur dike, so when the water depth is constant, the total

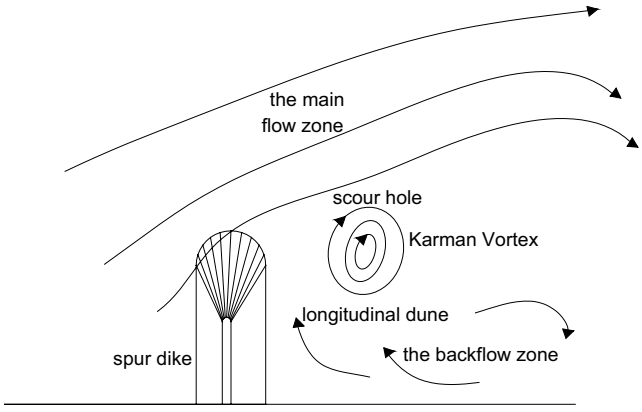

Fig. 7. Karman Vortex behind the spur dike end.

Table 1
Relationship between total pressure and discharge

Discharge (L/s)	Total pressure of sampling point						
	Upstream side			Spur dike end		Downstream side	
	2#4	3#7	4#1	5#4	6#7	7#7	8#4
25.8	0.996	1.001	0.675	0.759	0.745	0.854	0.930
38.7	0.987	0.997	0.644	0.735	0.719	0.809	0.882
51.0	0.978	0.992	0.579	0.681	0.665	0.764	0.826
68.0	0.987	1.004	0.529	0.469	0.378	0.432	0.441

pressure is mainly hydrostatic pressure. With the increase of discharge, the difference between upstream and downstream water levels increases, leading to the decrease of downstream water level with the increase of discharge. The results show that the hydrostatic pressure and total pressure decrease with the increase of flow rate.

As shown in Table 2 and Fig. 9, at each sampling point, the hydrodynamic pressure increases as the flow rate increases. When the water depth is constant, the larger the flow rate is, the stronger the turbulence intensity is, resulting in the increase of the pulsating pressure.

3.3.2. Influence of water depth on the force of spur dike

When Q = 38.7 L/s, l = 30 cm, and the water depth is 8, 10, and 12 cm, respectively, the stress conditions of 8 sampling points on the surface of the spur dike 1.67 cm from the bottom are compared and analyzed. The relationship between the total pressure of the spur dike and water depth is shown in Table 3 and Fig. 10. The relationship between fluctuating pressure and water depth is shown in Table 4 and Fig. 11.

It can be seen from Table 3 and Fig. 10, the total pressure on the spur dike basically increases linearly with the increase of water depth. This is because the total pressure is mainly hydrostatic pressure, which has a linear relationship with water depth.

It can be seen from Table 4 and Fig. 11 that at each sampling point, the hydrodynamic pressure decreases with the increase of water depth. When the flow rate is constant, the increase of water depth will lead to the increase of water passing area, the weakening of flow turbulence intensity and the decrease of hydrodynamic pressure.

3.3.3. Influence of the length on the stress of the spur dike

When Q = 38.7 L/s, H = 10 cm, and the length of the spur dike is 50, 30 and 20 cm, respectively, the stress of 8

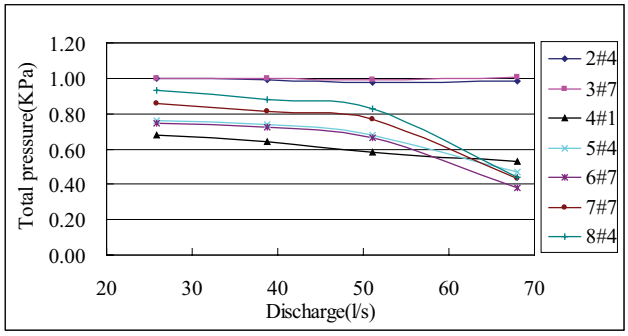

Fig. 8. Relationship between total pressure and discharge.

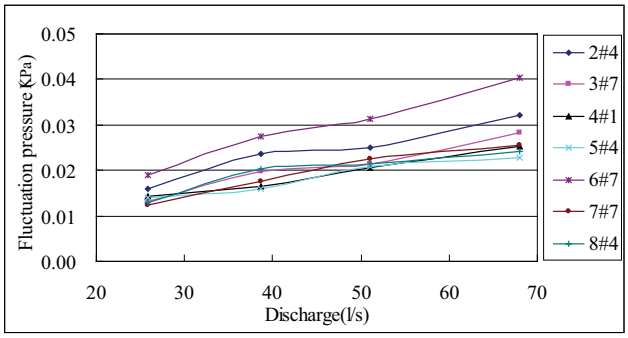

Fig. 9. Relationship between fluctuation pressure and discharge.

Table 2
Relationship between fluctuation pressure and discharge

Discharge (L/s)	Fluctuation pressure of sampling point						
	Upstream side			Spur dike end		Downstream side	
	2#4	3#7	4#1	5#4	6#7	7#7	8#4
25.8	0.015	0.013	0.014	0.013	0.019	0.012	0.012
38.7	0.023	0.019	0.016	0.016	0.027	0.017	0.020
51.0	0.024	0.021	0.020	0.021	0.031	0.022	0.021
68.0	0.032	0.028	0.025	0.022	0.040	0.025	0.024

Table 3
Relationship between total pressure and water depth

Water depth (cm)	Total pressure of sampling point						
	Upstream side			Spur dike end		Downstream side	
	2#4	3#7	4#1	5#4	6#7	7#7	8#4
8	0.779	0.790	0.419	0.448	0.447	0.535	0.609
10	0.987	0.997	0.644	0.735	0.719	0.809	0.882
12	1.186	1.190	0.857	0.957	0.950	1.048	1.123

Table 4
Relationship between fluctuation pressure and water depth

Water depth (cm)	Fluctuation pressure of sampling point						
	Upstream side		Spur dike end			Downstream side	
	2#4	3#7	4#1	5#4	6#7	7#7	8#4
8	0.023	0.020	0.017	0.033	0.029	0.029	0.026
10	0.023	0.019	0.016	0.016	0.025	0.017	0.020
12	0.018	0.014	0.014	0.012	0.012	0.013	0.014

Table 5
Relationship between total pressure and dike length

Dike length (cm)	Total pressure of sampling point						
	Upstream side		Spur dike end			Downstream side	
	2#4	3#7	4#1	5#4	6#7	7#7	8#4
20	0.761	0.756	0.683	0.709	0.705	0.702	0.708
30	0.987	0.997	0.694	0.735	0.719	0.809	0.882
50	0.934	0.826	0.541	0.643	0.567	0.590	0.600

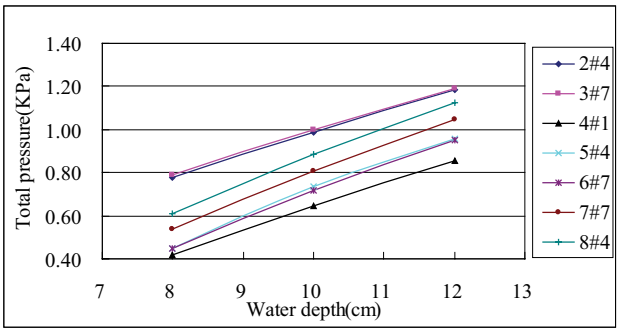

Fig. 10. Relationship between total pressure and water depth.

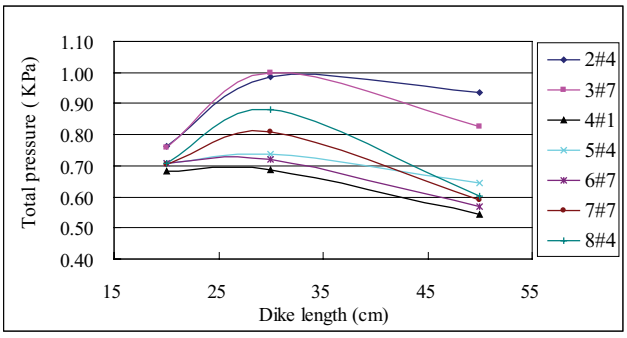

Fig. 12. Relationship between total pressure and dike length.

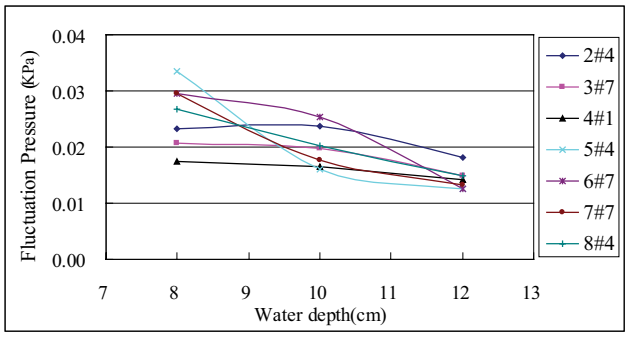

Fig. 11. Relationship between fluctuation pressure and water depth.

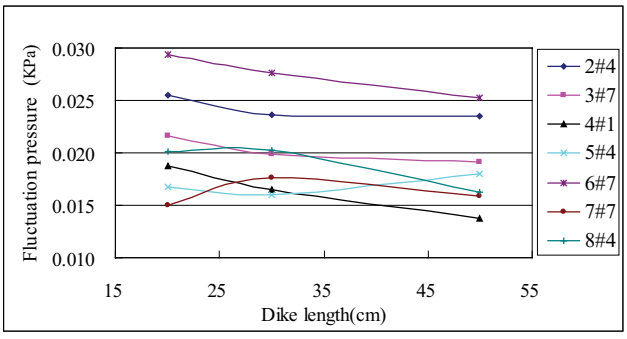

Fig. 13. Relationship between fluctuation pressure and dike length.

sampling points on the surface of the spur dike 1.67 cm from the bottom is compared and analyzed. The relationship between the total pressure of the spur dike and the length of the spur dike is shown in Table 5 and Fig. 12. The relationship between the hydrodynamic pressure and the length of the spur dike is shown in Table 6 and Fig. 13.

From Tables 5 & 6 and Figs. 12 & 13, it can be seen that the upstream total pressure of the spur dike is the largest,

Table 6
Relationship between fluctuation pressure and dike length

Dike length (cm)	Fluctuation pressure of sampling point						
	Upstream side			Spur dike end		Downstream side	
	2#4	3#7	4#1	5#4	6#7	7#7	8#4
20	0.025	0.021	0.018	0.016	0.029	0.015	0.020
30	0.023	0.019	0.016	0.016	0.027	0.017	0.020
50	0.023	0.019	0.013	0.018	0.025	0.015	0.016

the downstream total pressure is in the middle, and the end total pressure is the smallest. The total pressure at each sampling point increases first and then decreases with the increase of the length of the spur dike. At most sampling points, the hydrodynamic pressure decreases with the increase of the length of the spur dike.

4. Conclusions and discussion

The relationship between turbulence, force and scour around the spur dike was studied by flume generalized model experiment. The main conclusions are as follows: (1) There are strong flow turbulence and fluctuating pressure area behind the dike, and the area with the largest fluctuating kinetic energy and fluctuating pressure is almost the area with the most serious scour. (2) There is a single Karman Vortex behind the spur dike, and the relationship between the Karman Vortex and the back scour of the spur dike is explained. It is shown that the combined velocity of the approaching velocity and the vertex and edge linear velocity has a limiting effect on the back scour and the silting in the backflow area. (3) The total pressure on the spur dike decreases with the increase of discharge, water depth and length; The fluctuating pressure decreases with the increase of water depth and length of groin, and increases with the increase of discharge.

The current formulae for the depth of spur dike head can only be qualitative or cannot well meet the quantitative requirements, because these formulae all take the average flow velocity as the restriction factor of scour and ignore the strong turbulence of the water near the dike head and the existence of the whirlpool, which will affect the engineering design and construction to a certain extent. Therefore, the next research focus is to integrate these factors which have great influence on the scour of the dike head and try to improve the formula of the scour depth of the dike head.

Acknowledgment

Thanks to National Key Research and Development Program of China (Grant No. 2016YFC040210), National Natural Science Foundation (Grant No. 51079165) and Chongqing Frontier and Applied Basic Research Program of China (Grant No. cstc2015jcyjA30004). Thanks also go to the reviewers who provided valuable advices for the improvement of the manuscript.

References

[1] Q. Ying, Z.B. Jiao, Hydraulics of Spur Dike, Ocean Press, Beijing, 2004.
[2] J.H. Zhang, River Regulation and Embankment Management, Yellow River Conservancy Press, Zhengzhou, 1998.
[3] S.Y. Lim, Y.M. Chiew, Effect of sediment grain size on scour around the spur dike, Yangtze River, 25 (1994) 59–62.
[4] Q. Ying, A study on the local – scour holes at groin-nose, J. Nanchang Coll. Water Conserv. Hydroelectric Power, 18 (1999) 16–20.
[5] D.X. Fang, J. Wang, Study of initial scour velocity of bed sand around spur dike and computing model of local scour depth, J. Sediment Res., 4 (1992) 77–84.
[6] W.S.J. Uijttewaal, Effects of groyne layout on the flow in groyne fields: laboratory experiments, J. Hydraul. Eng., 131 (2005) 782–791.
[7] M.M. Mostafa, H.S.H. Ahmed, G.A.A. El-Raheem, N.A. Ali, Experimental Study on Flow Characteristics Around Single Groyne With Different Permeability in Compound Channel Flood Plain, 2013 IAHR Congress, Tsinghua University Press, Chengdu, China, 2013.
[8] H.S.H. Ahmed, M.M. Mostafa, G.A.A. El-Raheem, N.A. Ali, A. Tominaga, Flow analysis around groyne with different permeability in compound channel floodplains, J. Eng. Sci., 41 (2013) 302–320.
[9] B.Q. Xu, T. Yu, P.Y. Wang, X.W. Yang, X.F. Zhang, Experimental study on water surface line distribution of pervious groin in the upper reaches of the Yangtze River, J. Water Conserv. Water Transp. Eng., 5 (2019) 62–68.
[10] T. Yu, P.Y. Wang, L. Chen, Experimental study of the stability of spur dyke for different types, J. Appl. Sci., 203 (2013) 4040–4045.
[11] L. Zhong, S.C. Liao, J.M. Zhang, J.J. Liu, Turbulence characteristics of open channel flow with dense roughness bed, J. Sediment Res., 45 (2013) 8–14.
[12] W.E. Wang, W. Liao, L.J. Qi, Experimental study on flow turbulence characteristics of a wide and narrow channel, Adv. Water Sci., 31 (202) 394–403.
[13] A. Kumar, C.S.P. Ojha, Effect of different compositions in unsubmerged L-head groynes to mean and turbulent flow characteristics, KSCE J. Civ. Eng., 23 (2019) 4327–4338.
[14] Y. Chen, J. Li, H. Lu, P. Yan, Coupling system dynamics analysis and risk aversion programming for optimizing the mixed noise-driven shale gas-water supply chains, J. Cleaner Prod., 278 (2021) 123209, doi: 10.1016/j.jclepro.2020.123209.
[15] M.M. Bhatti, D.-Q. Lu, An application of Nwogu's Boussinesq model to analyze the head-on collision process between hydroelastic solitary waves, Open Phys., 17 (2019) 177, doi: 10.1515/phys-2019-0018.
[16] C. Zhang, J. Ou, Control structure interaction of electromagnetic mass damper system for structural vibration control, J. Eng. Mech., 134 (2008) 428, doi: 10.1061/(ASCE)0733-9399(2008)134:5(428).
[17] H. Lu, P. Tian, L. He, Evaluating the global potential of aquifer thermal energy storage and determining the potential worldwide hotspots driven by socio-economic, geo-hydrologic and climatic conditions, Renewable Sustainable Energy Rev., 112 (2019) 788–796.

[18] X. Hu, P. Ma, B. Gao, M. Zhang, An integrated step-up inverter without transformer and leakage current for grid-connected photovoltaic system, IEEE Trans. Power Electron., 34 (2019) 9814, doi: 10.1109/TPEL.2019.2895324.
[19] S. Liu, X. Zhang, F. Gao, L. Wei, Q. Liu, H. Lü, B. Wang, Two-dimensional flow field distribution characteristics of flocking drainage pipes in tunnel, Open Phys., 18 (2020) 139, doi: 10.1515/phys-2020-0013.
[20] X. Wang, X. Lyu, Experimental study on vertical water entry of twin spheres side-by-side, Ocean Eng., 221 (2021) 108508, doi: 10.1016/j.oceaneng.2020.108508.
[21] L. Cao, C. Tu, P. Hu, S. Liu, Influence of solid particle erosion (SPE) on safety and economy of steam turbines, Appl. Therm. Eng., 150 (2019) 552–563.